JCI The Journal of Clinical Investigation

Macrophage AXL receptor tyrosine kinase inflames the heart after reperfused myocardial infarction

Matthew DeBerge, … , Ira Tabas, Edward B. Thorp

J Clin Invest. 2021. https://doi.org/10.1172/JCI139576.

Research In-Press Preview Cardiology Inflammation

Graphical abstract

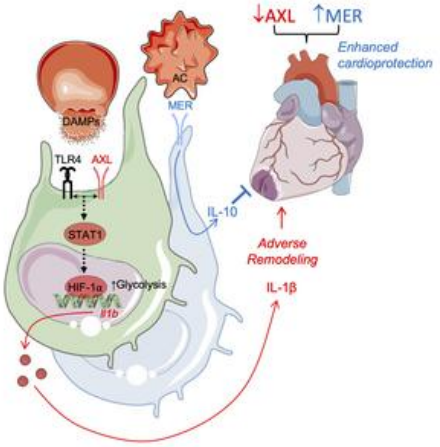

Find the latest version:

https://jci.me/139576/pdf

MACROPHAGE AXL RECEPTOR TYROSINE KINASE INFLAMES THE HEART AFTER REPERFUSED MYOCARDIAL INFARCTION

Matthew DeBerge[1,2], Kristofor Glinton[1,2], Manikandan Subramanian[3], Lisa D Wilsbacher[2,4], Carla V Rothlin[5], Ira Tabas[6], Edward B. Thorp[1,2]

[1]Department of Pathology, Feinberg School of Medicine, Northwestern University, Chicago, IL, USA

[2]Feinberg Cardiovascular & Renal Research Institute, Feinberg School of Medicine, Northwestern University, Chicago, IL, USA

[3]William Harvey Research Institute, Barts and The London School of Medicine and Dentistry, Queen Mary University of London, London, United Kingdom

[4]Department of Medicine, Feinberg School of Medicine, Northwestern University, Chicago, IL, USA

[5]Department of Immunobiology, Yale School of Medicine, New Haven, CT, USA

[6]Department of Medicine, Department of Pathology and Cell Biology, and Department of Physiology, Columbia University Irving Medical Center, New York City, NY, USA

Address Correspondence: Edward B Thorp, 300 East Superior St, Tarry 3-705, Chicago, IL 60611, 312-503-4309, ebthorp@northwestern.edu

The authors have declared that no conflict of interest exists.

ABSTRACT

Tyro3, AXL, and MerTK (TAM) receptors are activated in macrophages in response to tissue injury and as such have been proposed as therapeutic targets to promote inflammation resolution during sterile wound healing, including myocardial infarction. While the role of MerTK in cardioprotection is well-characterized, the unique role of the other structurally similar TAMs, and particularly AXL, in clinically-relevant models of myocardial ischemia-reperfused infarction (IRI) is comparatively unknown. Utilizing complementary approaches, validated by flow cytometric analysis of human and murine macrophage subsets and conditional genetic loss and gain of function, we uncover a unique maladaptive role for myeloid AXL during IRI in the heart. Cross signaling between AXL and TLR4 in cardiac macrophages directed a switch to glycolytic metabolism and secretion of proinflammatory IL-1β, leading to increased intramyocardial inflammation, adverse ventricular remodeling, and impaired contractile function. AXL functioned independently of cardioprotective MerTK to reduce the efficacy of cardiac repair, but like MerTK, was proteolytically cleaved. Administration of a selective small molecule AXL inhibitor alone improved cardiac healing, which was further enhanced in combination with blockade of MerTK cleavage. These data support further exploration of macrophage TAM receptors as therapeutic targets for myocardial infarction.

INTRODUCTION

Myocardial infarction (MI) is a leading cause of heart failure and is associated with an increased risk of death. Intramyocardial inflammation arising after cardiomyocyte cell death from reperfused infarction contributes to pathological cardiac remodeling and progression to heart failure (1, 2). Phagocytes within the heart, particularly macrophages, recognize damage-associated molecular patterns (DAMPs) released by dying cardiomyocytes, which triggers pathological inflammatory responses (3). Although results from clinical trials with broad immunosuppression have failed to show any effect (4), specific targeting of proinflammatory cytokines has conferred clinical benefits (2). Recent results from the Canakinumab Anti-Inflammatory Thrombosis Outcome Study (CANTOS) (5), which targeted the inflammatory cytokine, interleukin (IL)-1β, demonstrated the merits of a targeted approach, as opposed to generalized immunosuppression, in reducing recurrent cardiovascular events in patients with ischemic cardiomyopathy, albeit with a compromise in host defense.

Macrophages express a family of receptor tyrosine kinases, Tyro3, AXL, MerTK (TAM), that mediate the clearance of apoptotic cells (efferocytosis), regulate inflammatory cytokine production, and in the case of MerTK, mediate resolution of inflammation (6-9). While the role of *Mertk*- and *phagocytosis*-dependent cardiac repair after myocardial infarction is well characterized (10-12), less is known about the role of other TAM receptors in tissue repair after myocardial injury. AXL protein expression is increased in myocardial biopsies of patients with end-stage heart failure (13). Moreover, the extracellular domain of AXL is proteolytically cleaved, which releases a stable product called soluble AXL (solAXL), and there is a correlation among elevated solAXL, heightened markers of inflammation, and poor prognosis during heart failure (13, 14). However, whether AXL or its cleavage regulates the initial inflammatory and reparative

macrophage responses in a manner that affects disease progression, either positively or negatively, requires investigation.

To ascertain the role of macrophage AXL and AXL cleavage during ischemic tissue injury, we examined cardiac repair in mice genetically engineered to lack AXL or to be resistant to AXL cleavage. Our findings reveal that AXL, in contrast to MerTK, antagonizes optimal cardiac repair by promoting a switch to glycolytic metabolism in macrophages to fuel proinflammatory responses and that AXL cleavage is a mitigating factor in this process.

RESULTS

We first evaluated AXL expression on myeloid cells in mice subjected to a clinically-relevant model of myocardial ischemia-reperfused infarction (IRI). Both gene and protein expression of AXL was detected in a subset of cardiac macrophages expressing high levels of major histocompatibility complex II (MHCII^{HI}) (Figure 1A, Supplemental Figure 1A, 1B). Survey of tissue resident macrophages across various tissues demonstrated widespread expression of AXL on macrophages, with preferential AXL expression on MHCII^{HI} subsets in a variety of tissues, including the peritoneum and liver (Supplemental Figure 2), consistent with data assembled by the ImmGen consortium (15) and previous reports (16, 17). In contrast, AXL protein expression was not detectable on either neutrophils or Ly6C^{hi} monocytes (Supplemental Figure 1C, 1 D), indicating that MHCII^{HI} cardiac macrophages were a major source for myeloid cell AXL in the heart. Following IRI, AXL expression was increased on infarct-associated MHCII^{HI} cardiac macrophages and remained significantly increased through the progression to heart failure 30 days after IRI (Figure 1B). Thus, macrophage AXL expression persists after IRI through the progression to heart failure. Moreover, a relative high level of AXL expression was detected in macrophages obtained from peri-infarct tissue of explanted hearts in patients with ischemic cardiomyopathy (Figure 1C, Supplemental Figure 3).

To determine the causal functional role of AXL expression in cardiac macrophages in the acute phase after IRI, we compared left ventricular (LV) remodeling and contractile function between *Axl+/+* and *Axl-/-* mice after IRI. Pathological measurements of infarct size 7 days after IRI revealed smaller sized infarcts in *Axl-/-* mice compared to *Axl+/+* mice (Figure 2A). Despite similar baseline echocardiographic parameters, *Axl*-deficiency resulted in greater preservation of LV systolic function 21 days after IRI compared to *Axl+/+* mice (Figure 2B). Given that AXL is also expressed on non-myeloid cells, including endothelial cells and dendritic cells (18, 19), we performed IRIs on lethally-irradiated wild-type recipients of *Axl*-deficient bone marrow or in mice with selective *Axl* deletion in myeloid cells (*LysM-Cre*$^{+}$*Axl*^{flox} mice) (Figure 2C). Similar to whole body knockouts, myeloid-specific deletion of *Axl* resulted in significantly smaller infarcts 7 days after IRI compared to controls (Figure 2D, Supplemental Figure 4A) and these results extended to both female mice and a small cohort of male mice (Supplemental Figure 4B). Since *LysM-Cre*-mediated recombination results in *Axl* deletion predominantly among monocytes, neutrophils, and macrophages and AXL was not detected on monocytes and neutrophils, these results suggest AXL acts in macrophages to exacerbate cardiac repair after IRI.

We next investigated whether *Axl*-deficiency impacted the extent and quality of immune cell infiltrate in the heart after IRI. Using flow cytometry, we found that *Axl*-deficiency did not affect initial neutrophil and Ly6C^{hi} monocyte recruitment to the infarcted myocardium (Figure 3A, 3B). However, by 3 days after IRI, there was a significant reduction in the total number of neutrophils and Ly6C^{hi} monocytes in *Axl-/-* mice compared to *Axl+/+* mice (Figure 3A, 3B). Importantly, similar total number of neutrophils and Ly6C^{hi} monocytes were observed in the periphery of *Axl+/+* and *Axl-/-* mice at both baseline and after IRI (Supplemental Figure 5), consistent with a role for AXL in amplifying local cardiac inflammation. While no differences were observed in the total number of macrophages in the infarcted myocardium after IRI (Figure 3C), there was an increase in

macrophage polarization towards a reparative phenotype in *Axl-/-* mice compared to *Axl+/+* mice as measured by an increase in the ratio of MHCII^{LO} to MHCII^{HI} cardiac macrophages (Figure 3D). We and others have shown that MHCII^{LO} cardiac macrophages secrete higher levels of IL-10 to restrain inflammation and fibrosis (12, 20), while MHCII^{HI} cardiac macrophages are enriched in genes regulating the NLRP3 inflammasome (21), which regulates IL-1β secretion. Despite similar baseline levels, we observed increased expression of anti-inflammatory genes, *Il10* and *Tgfb*, and decreased proinflammatory genes, *Il1b*, *Il6*, and *Tnf*, within cardiac extracts (Figure 3E), as well as decreased IL-1β and increased IL-10 levels in the serum of *Axl-/-* mice compared to *Axl+/+* mice (Figure 3F). Similar to whole body knockouts, myeloid-specific deletion of *Axl using* *LysMCre^{+}Axl^{flox}* mice resulted in increased reparative MHCII^{LO} macrophages, which was associated with a decrease in inflammatory neutrophils and monocytes within the infarct and reduced serum levels of IL-1β (Supplemental Figure 6). *Axl*-deficiency also favored MHCII^{LO} macrophage polarization in a model of peritonitis (Supplemental Figure 7), suggesting that AXL signaling promotes inflammatory reprogramming of macrophages in a variety of inflammatory settings.

Next, we explored how AXL signaling in macrophages promoted inflammatory reprogramming after IRI. To assess macrophage polarization, we examined proinflammatory gene expression in bone marrow-derived macrophages (BMDMs) from *Axl+/+* and *Axl-/-* mice after stimulation of toll-like receptor 4 (TLR4), which recognizes DAMPs released by dying cardiomyocytes (22). Similar to our findings in vivo, *Axl*-deficiency attenuated expression of proinflammatory genes, including *Il1b* and *Tnf*, and increased anti-inflammatory *Il10* in BMDMs after TLR4 stimulation without affecting baseline gene levels (Figure 4A). Importantly, both *Axl+/+* and *Axl-/-* BMDMs expressed similar levels of TLR4 (Figure 4B). Given the recent success in targeting IL-1β to reduce recurrent myocardial infarctions in ischemic cardiomyopathy patients (5), we performed additional

experiments to investigate the relationship between AXL signaling and macrophage production of IL-1β. In serum-starved BMDMs, addition of AXL-specific agonists, including either growth arrest-specific 6 (Gas6) or an agonizing antibody, increased TLR4 priming of the inflammasome as measured by increased *Il1b* expression in *Axl*+/+ BMDMs, but these effects were absent from *Axl-/-* BMDMs (Figure 4C). Furthermore, inflammasome activation with ATP was also impaired by *Axl*-deficiency as measured by a reduction in both activated Caspase-1 (Figure 4D, 4E) and secretion of IL-1β into the culture media (Figure 4F), supporting the concept that AXL signaling augments TLR4 priming of the NLRP3 inflammasome. Impaired inflammatory activation in *Axl-/-* BMDMs was also evidenced by a decrease in TNF-α levels with a concomitant increase in IL-10 levels after TLR4 stimulation (Figure 4G, 4H).

Macrophages activated by TLR4 signaling require a switch to glycolytic metabolism to facilitate the increased energetic demands necessary to produce IL-1β (23). To determine whether AXL signaling was required for inflammatory glycolytic reprogramming, we measured the extracellular acidification rate of *Axl+/+* and *Axl-/-* BMDMs after TLR4 stimulation. While we observed an increase in glycolysis in *Axl+/+* BMDMs after TLR4 stimulation, this effect was largely absent in *Axl-/-* BMDMs (Figure 5A). AXL signaling alone, using an AXL agonizing antibody, was also sufficient to promote an increase in glycolysis compared to an isotype control, albeit to a lesser extent than TLR4 stimulation (Figure 5B). To test whether AXL and TLR4 can be in spatial proximity to promote inflammatory glycolytic reprogramming, we performed a proximity ligation assay. While the assay revealed data consistent with a close interaction between AXL and TLR4 in BMDMs (Supplemental Figure 8A), no differences in NF-κB signaling were observed between *Axl+/+* and *Axl-/-* BMDMs after TLR4 stimulation (Supplemental Figure 8B), suggesting that AXL augmented glycolysis independent of NF-κB activation. Hypoxia inducible factor 1α (HIF-1α) has been implicated in the TLR4-mediated switch to glycolytic metabolism (24), so we next

investigated whether *Axl*-deficiency impacted HIF-1α activation. Relative to *Axl+/+* BMDMs, there were reductions in both gene and protein expression of HIF-1α in *Axl-/-* BMDMs (Figure 5C, 5E, 5F), which was associated with a decrease in HIF-1α-dependent genes involved in glycolytic metabolism (Figure 5D). Treatment of BMDMs with cobalt chloride, a pharmacological HIF activator, restored glycolytic metabolism in *Axl-/-* BMDMs to a level similar to that of *Axl+/+* BMDMs (Figure 5G), suggesting that AXL signaling is required for HIF-1α-dependent glycolytic proinflammatory reprogramming of macrophages in response to inflammatory stimuli.

AXL signaling promotes phosphorylation and activation of STAT1 (7, 18), which has been separately linked to both HIF-1α signaling (25) and IL-1β production (26). To test whether AXL was required for STAT1 signaling after TLR4 stimulation, we measured phosphorylation of STAT1 (pSTAT1, Tyr701) in BMDMs after TLR4 stimulation or in cardiac macrophages after IRI. Treatment of *Axl+/+* BMDMs with the AXL specific agonist, Gas6, revealed that while Gas6-AXL signaling alone was sufficient to induce pSTAT1, it was insufficient to increase glycolytic metabolism or IL-1β production (Supplemental Figure 9). TLR4 stimulation also increased pSTAT1 levels in *Axl+/+* BMDMs (Figures 6A, 6B) and the addition of exogenous Gas6 augmented both pSTAT1 levels and IL-1β production during TLR4 stimulation (Supplemental Figure 9). In contrast, pSTAT1 levels were attenuated in *Axl-/-* BMDMs after TLR4 stimulation (Figures 6A, 6B). Similarly, pSTAT1 levels were reduced after IRI in cardiac macrophages from *Axl-/-* mice compared to *Axl+/+* mice (Figure 6C), supporting a crucial role for AXL in STAT1 activation. To test whether STAT1 signaling was required for TLR4-mediated glycolytic proinflammatory reprogramming of macrophages, we measured metabolic and inflammatory function in *Stat1+/+* and *Stat1-/-* BMDMs after TLR4 stimulation. In contrast to *Stat1+/+* BMDMs, HIF-1α activation was attenuated in *Stat1-/-* BMDMs after TLR4 stimulation (Figure 6D), which was associated with an impaired switch to glycolytic metabolism (Figure 6E) and reduced

secretion of IL-1β (Figure 6F). Taken together, these results support a role for Gas6-AXL signaling in augmenting TLR4 activation of HIF-1α through STAT1 signaling to promote the glycolytic reprogramming to inflammatory macrophages.

As cardiac macrophages express AXL and MerTK, both of which are efferocytosis receptors, one hypothesis is that in addition to impairing proinflammatory macrophage reprogramming, loss of AXL would improve cardiac repair through increased cardioprotective MerTK-dependent phagocytic clearance of apoptotic cardiomyocytes. To test whether enhanced efferocytosis restrained inflammation and improved cardiac repair in *Axl-/-* mice, we quantified post-IRI association of fluorescent and cardiomyocyte-specific mCherry protein with cardiac macrophages. While IRI led to significantly increased macrophage clearance of cardiomyocyte debris, no difference in reperfusion-dependent efferocytosis of dead cardiomyocytes was observed between *Axl+/+* and *Axl-/-* mice (Figure 7A). The phagocytosis-independent cardioprotection observed during *Axl*-deficiency suggests that AXL and MerTK function independently to regulate reprogramming of macrophages.

We next tested whether AXL and MerTK exhibited divergent and independent function after IRI by comparing LV remodeling and contractile function in mice deficient in either receptor alone or deficient in both AXL and MerTK. In contrast to loss of AXL alone, loss of MerTK alone worsened cardiac repair and contractile function after IRI (Figure 7B), as previously reported by us and others (11, 12). Importantly, loss of either AXL or MerTK did not result in a compensatory increase in the other receptor on cardiac macrophages (Figure 7C). Surprisingly, mice deficient in both *Axl* and *Mertk* exhibited a cardioprotective response after IRI similar to mice deficient in *Axl* alone, with improvements in cardiac repair and preservation of systolic function compared to controls or mice deficient in *Mertk* alone (Figure 7B, 7D). Flow cytometric analyses revealed an increase in

reparative MHCII^{LO} cardiac macrophages in *Axl-/-Mertk-/-* mice compared to *Axl+/+Mertk+/+* mice after IRI (Figure 7E), suggesting that AXL favors accumulation of proinflammatory MHCII^{HI} macrophages to worsen cardiac repair after IRI. Taken together, these results support divergent roles for AXL and MerTK in mediating pathogenic and protective macrophage responses, respectively, after IRI.

To test the therapeutic potential of these findings, we treated mice daily after IRI with a small molecule inhibitor for AXL, R428, that binds specifically (IC_{50}=14nM) and with high selectivity to the AXL intracellular catalytic kinase domain and inhibits its activity (50-fold relative to MerTK) (27). Treatment of WT mice with the AXL inhibitor significantly reduced infarct size, demonstrating that transient inhibition of AXL confers cardioprotection after IRI (Figure 7F). Similar cardioprotection was observed following administration of AXL inhibitor to *Mertk-/-* mice after IRI (Figure 7G), consistent with independent functions for AXL and MerTK in the infarcted ventricle. We have previously shown that the beneficial effects of MerTK are compromised by its proteolytic cleavage after IRI and that strategies that block reperfusion-associated MerTK cleavage improve cardiac function (12). To test whether targeting both AXL and MerTK could synergize to enhance cardiac repair after IRI, we treated mice with a cleavage resistant MerTK (*MertkCR/CR*), which preserves the cardioprotective effects naturally compromised after IRI, with the AXL-specific inhibitor. Treatment of *MertkCR/CR* mice with AXL inhibitor reduced infarct size compared to either intervention alone (Figure 7F), demonstrating that strategies that combine inhibition of AXL signaling and MerTK cleavage may confer the greatest preservation of cardiac function after IRI.

Similar to MerTK, AXL is also proteolytically cleaved to release a stable cleavage product called solAXL. In ST-segment elevation myocardial infarction (STEMI) patients, solAXL levels are increased during the acute phase and are associated with adverse ventricular remodeling and progression to heart failure (14). We independently validated this finding in a small cohort of

STEMI patients and observed a similar increase in serum levels of solAXL in mice after IRI (Supplemental Figure 10A, 10B). To test the role of AXL cleavage after IRI, we generated gene-targeted mice (*Axl*$^{CR/CR}$) in which the proteolysis site of AXL was deleted, leading to replacement of the wild-type AXL with a fully functional but cleavage-resistant AXL (Supplemental Figure 11A-D). To assess cleavage resistance, BMDMs from *Axl*$^{CR/CR}$ and *Axl*$^{+/+}$ mice were treated with a TLR4 agonist and then assayed for cell-surface AXL and solAXL by flow cytometry, ELISA, and immunoblot. TLR4 agonism decreased cell-surface AXL and increased solAXL in *Axl*$^{+/+}$ macrophages, but these effects were largely absent with *Axl*$^{CR/CR}$ macrophages (Figure 8A, 8B, Supplemental Figure 11E). Consistent with a role for AXL in the proinflammatory metabolic reprogramming of macrophages, we observed increased pSTAT1 and HIF-1α signaling in *Axl*$^{CR/CR}$ BMDMs compared to *Axl*$^{+/+}$ BMDMs (Figure 8C, 8D), which was associated with elevated glycolysis and IL-1β secretion in response to TLR4 stimulation (Figure 8E, 8F). In *Axl*$^{CR/CR}$ mice, cell surface AXL was preserved on cardiac macrophages after IRI (Figure 9A) and serum solAXL was significantly reduced at both steady-state and after IRI compared to *Axl*$^{+/+}$ mice (Figure 9B). In contrast to the increase in solAXL levels observed in *Axl*$^{+/+}$ mice after IRI, *Axl*$^{CR/CR}$ mice exhibited no change in solAXL levels after IRI validating the *Axl*$^{CR/CR}$ mouse as a model for testing the functional consequences of AXL cleavage in vivo. To determine the functional role of AXL cleavage in the acute phase after IRI, we compared inflammation and tissue repair between *Axl*$^{+/+}$ and *Axl*$^{CR/CR}$ mice after IRI. Relative to *Axl*$^{+/+}$ mice, infarct sizes were increased in *Axl*$^{CR/CR}$ mice 7 days after IRI (Figure 9C). The adverse ventricular remodeling in *Axl*$^{CR/CR}$ mice was associated with an increased inflammatory response as measured by increased neutrophils (Figure 9D), Ly6C^{hi} monocytes (Figure 9E), and inflammatory MHCII^{HI} macrophages (Figure 9F) within the infarct and elevated serum levels of IL-1β (Figure 9G) compared to *Axl*$^{+/+}$ mice, revealing that AXL cleavage limits adverse ventricular remodeling after IRI.

DISCUSSION

Our data reveal a role for AXL in adverse cardiac remodeling after IRI. According to our working model (Supplemental Figure 12), release of DAMPs secondary to IRI promotes increased AXL levels on cardiac macrophages. Cross signaling between AXL and TLR4 augments STAT1 signaling to direct a HIF-1α-dependent switch to glycolytic metabolism in cardiac macrophages and secretion of proinflammatory IL-1β. This leads to increased intramyocardial inflammation and culminates in adverse ventricular remodeling and impaired contractile function. AXL functions independently of cardioprotective MerTK to worsen cardiac repair, but like MerTK, is proteolytically cleaved. Finally, administration of a selective small molecule inhibitor of AXL alone reduced cardiac damage. AXL inhibition in combination with blockade of MerTK cleavage further improved cardiac healing after IRI. This interesting AXL-MerTK dichotomy strengthens the foundation to investigate macrophage TAM receptors as targets for cardioprotection in the infarcted human heart.

While a proinflammatory role for AXL in cardiac macrophages was somewhat surprising, given its well-characterized role in efferocytosis (28), emerging evidence from both humans and experimental models is beginning to support a detrimental role for AXL in a variety of diseases (29, 30). In our model of clinically-relevant myocardial IRI, we observed both increased serum levels of solAXL and cell-surface AXL expression on cardiac macrophages, the latter which promoted proinflammatory IL-1β production. Using a newly generated cleavage-resistant AXL mouse, we discovered that the increase in solAXL by proteolytic cleavage of cell-surface AXL functioned to limit proinflammatory macrophage responses in vitro and adverse ventricular remodeling during the acute phase after IRI. AXL expression on cardiac macrophages remained elevated after IRI into the progression to heart failure, consistent with the AXL expression we detected on cardiac macrophages during ischemic cardiomyopathy and the increased AXL

expression observed in myocardial extracts from heart failure patients (13). Elevated levels of the AXL ligand, Gas6, have also been observed in heart failure patients (14).

A survey of tissue resident macrophages in a variety of tissues revealed widespread expression of AXL on macrophages throughout the body, consistent with macrophage profiles within the ImmGen databases. In addition to its inflammatory role in the heart, we found that AXL regulated macrophage polarization during peritonitis, supporting the concept that AXL regulation of proinflammatory reprogramming is a conserved mechanism that may be translatable to macrophages in other inflammatory conditions, although this effect is likely to be context-dependent. For example, during acute viral infection in the lung, AXL functions by clearing apoptotic cells to resolve inflammation and mediate tissue repair (31), which may subsequently impair the host response to a secondary infection (32). In contrast, models of sterile tissue injury in the lung (33) and liver (29) have demonstrated that AXL promotes detrimental tissue fibrotic responses. These previous studies relied on global deletion or blockade of AXL and given that *Axl* gene expression is not restricted to macrophages and is active on other cell types, including endothelial cells, fibroblasts, and dendritic cells, it is unclear whether the varied outcomes reflect the cumulative inhibition of cell-specific AXL protein function. In our studies, we leveraged mice with specific deletion of *Axl* within the myeloid compartment and found that *Axl* deletion in macrophages recapitulated many of our findings in mice with global *Axl* deletion, revealing a direct role for AXL in macrophage inflammation after reperfused infarction.

AXL signaling in macrophages exacerbated myocardial inflammation through augmentation of TLR4 signaling to enhance proinflammatory IL-1β production. TLR4 is known to cross signal with other receptor tyrosine kinases, including the epidermal growth factor receptor (EGFR) (34), which is required for TLR4-dependent downstream signaling cascades that lead to proinflammatory cytokine production. Furthermore, there is considerable overlap between AXL

signaling cascades and canonical TLR4 downstream effectors, including NF-κB, PI3k/Akt, and TBK1 (35-37), suggesting that the molecular mechanisms regulating crosstalk between AXL and TLR4 select for specific downstream effectors to determine functional outcomes. While a proximity ligation assay suggested close protein interactions between AXL and TLR4, AXL was dispensable for NF-κB signaling after TLR4 stimulation in macrophages. Instead, AXL augmented STAT1 activation after TLR4 stimulation to direct a HIF-1α-dependent switch to glycolytic metabolism in cardiac macrophages, and secretion of proinflammatory IL-1β. Both STAT1 and HIF-1α have been linked to M1 macrophage activation within the M1/M2 macrophage polarization paradigm (38), supporting an upstream role for AXL in the activation of inflammatory macrophage polarization after TLR4 stimulation. This was in contrast to a previous report which found AXL signaling in peritoneal macrophages inhibited IL-1β through autophagy induction (39). However, this inhibitory effect was independent of STAT1 signaling. This suggests our findings in bone marrow-derived macrophages in vitro and cardiac macrophages in vivo represent a separate and distinct pathway. Interestingly, HIF-1α has been shown to directly regulate *Axl* expression in cancer cells (40), suggesting a putative mechanism where AXL activation in cardiac macrophages during the acute phase after reperfused infarction stabilizes HIF-1α to further enhance AXL-dependent inflammatory macrophage responses and promote heart failure progression.

The maladaptive role of AXL contrasts with the cardioprotective role of fellow TAM member MerTK in the infarcted heart, consistent with AXL and MerTK differentially regulating cardiac macrophage function. In support of opposing roles for AXL and MerTK, previous studies have revealed protective and detrimental roles for MerTK and AXL, respectively, at the tissue level in experimental models of immune-mediated nephritis (41) and chronic liver disease (16). Here, we report at the cellular level that AXL signaling promotes proinflammatory macrophage activation as *Axl*-deficiency reduced proinflammatory MHCII^{HI} cardiac macrophages after IRI. Similar to

macrophages within atherosclerotic lesions (42), this occurred independent to changes in efferocytosis, as AXL was dispensable for macrophage efferocytosis of apoptotic cardiomyocytes after IRI. Macrophage polarization is linked to metabolic reprogramming and we found that AXL was required for the switch to glycolytic metabolism to fuel inflammatory responses. In contrast, MerTK is required for anti-inflammatory macrophage reprogramming as *Mertk*-deficiency skews cardiac macrophages from an anti-inflammatory $MHCII^{LO}$ to proinflammatory $MHCII^{HI}$ phenotype (12). While macrophages leverage efferocytic metabolites to fuel mitochondrial metabolism and anti-inflammatory reprogramming (43), whether MerTK is linked to this metabolic reprogramming is the subject of future investigations. Taken together, the divergent role for AXL and MerTK in cardiac macrophages within the infarcted heart has important implications for the study of TAM receptors in both homeostasis and disease. Many studies have employed mice deficient in both *Axl* and *Mertk*, which may yield equivocal results if one receptor dominates the phenotype or the receptors diverge in function. Our results necessitate examining TAM receptor function both in isolation and combination.

In a therapeutic context, our findings suggest that clinical AXL inhibition in the acute phase after MI may reduce inflammation and adverse ventricular remodeling after MI to limit the progression to heart failure. The link between AXL and macrophage secretion of proinflammatory IL-1β indicates that AXL inhibition may be an interesting alternative to canakinumab, the monoclonal antibody targeting IL-1β that demonstrated efficacy in reducing recurrent cardiovascular events in humans but failed to gain approval for cardiovascular disease indications. The specific and highly selective AXL inhibitor used in our studies is orally bioavailable and has demonstrated favorable safety profiles and activity over prolonged periods of administration in clinical trials for the treatment of cancer in humans (44). Targeted delivery of an AXL inhibitor to cardiac macrophages during the perioperative period would circumvent the differential role AXL may exert

in different myocardial cell populations. However, our data in whole body *Axl* knockouts and mice treated with the AXL inhibitor suggests that transient inhibition of AXL confers protection with minimal off target effects. While simultaneous inhibition of AXL signaling and preservation of MerTK function led to greater cardioprotection, AXL may exert dominance over MerTK in the response to IRI, as combined loss of *Axl* and *Mertk* or treatment of *Mertk*-deficient mice with the AXL inhibitor improved cardiac repair. Given the potential dominance of AXL over MerTK and the relative ease in therapeutic targeting of AXL compared to MerTK cleavage, strategies that inhibit AXL may yield more immediate clinical benefits in cardiovascular disease.

In conclusion, our findings reveal that AXL aggravates cardiac repair by directing proinflammatory metabolic reprogramming of macrophages and that the mechanism is distinct from MerTK, the latter of which is necessary for macrophage efferocytosis of apoptotic cardiomyocytes to initiate inflammation resolution. These findings support exploration of leveraging macrophage TAM receptors in humans to promote inflammation resolution and limit adverse ventricular remodeling that leads to heart failure.

METHODS

Human Ischemic Cardiomyopathy Specimens: This study was approved by the Institutional Review Board at Northwestern University (#STU00012288) and performed in accordance with the Helsinki Doctrine on Human Experimentation. Written consent was obtained from all study participants. Cardiac tissue specimens were obtained from the explanted hearts of adult patients with ischemic cardiomyopathy undergoing cardiac transplantation at Northwestern Memorial Hospital. Explanted hearts were immediately immersed and rinsed with cold cardioplegia solution. Tissue specimens from infarct-scar or viable remote (absence of fibrosis) myocardium were obtained from the lateral wall of the left ventricle. Specimens were maintained in cold cardioplegia solution to preserve tissue integrity. Within 1 hour of procurement, specimens were digested with collagenase type II (600U/ml, Worthington) and DNase I (0.1mg/ml) in HBSS at 37°C for 30 minutes with agitation. Specimens were subsequently triturated through a 40μm cell strainer to prepare a single cell suspension for analyses by flow cytometry.

Human ST-segment elevation MI Plasma Specimens: This study was approved by the Institutional Review Board at Northwestern University (#STU00075325) and performed in accordance with the Helsinki Doctrine on Human Experimentation. Written consent was obtained from all study participation and subjects were excluded from the study if they were pregnant or unable to consent. Human peripheral blood was collected in BD Vacutainer EDTA-coated tubes (lavender top) from healthy controls or patients diagnosed with ST-segment elevation MI via electrocardiography within 24 hours of being admitted to the cardiac care unit at Northwestern Memorial Hospital. Blood was centrifuged at 5,000 rpm for 15 minutes 4°C to remove cells and platelets and plasma was stored at -80°C until analyses. Levels of soluble AXL in diluted plasma (1:100) were measured by ELISA according to the manufacturer's instructions. Absorbances were read at 450 nm on an iMark Microplate Reader (BIO-RAD).

Mice: *C57BL/6J* mice were bred in our animal facility prior to use as wild-type controls. *MerKD* (referred to herein as *Mertk-/-*), cleavage-resistant MerTK (*MertkCR/CR*), and *Axl-/-* mice have been previously described (12, 45, 46) and were backcrossed to *BL/6J* for ten generations. *Mertk-/-* and *Axl-/-* mice were crossed to generate mice double-deficient in *Mertk* and *Axl* (*Axl-/-Mertk-/-*). *LysM-Cre* (B6.129P2-Lyz2$^{tm1(cre)Ifo}$/J, Stock No: 004781), αMHC-mCherry (Tg(Myh6*-mCherry)2Mik, Stock No: 021577), and *Stat1-/-* (B6.129S(Cg)-Stat1^{tm1Dlv}/J, Stock No: 012606) mice were purchased from Jackson Laboratories. *Axl^{flox}* mice were generated in *BL/6J* background as previously described (19) and provided by Dr. Carla Rothlin (Yale University). *Axl^{flox}* mice were crossed with mice expressing *LysM-Cre* to generate mice with specific deletion of *Axl* in myeloid cells (*LysM-Cre^{+}Axl^{flox}* mice). *Axl^{flox}* littermates without *LysM-Cre* were used as controls in experiments with *LysM-Cre^{+}Axl^{flox}* mice. Mice were housed in temperature- and humidity-controlled, pathogen-free environments and kept on a 14:10h day/night cycle with access to standard mouse chow and water *ad libitum*. Two- to four-month old female or male mice were used for experiments. Animal studies were conducted in accordance with guidelines using a protocol approved by the Institutional Animal Care and Use Committee at Northwestern University.

AXL cleavage resistant mice: Cleavage resistant AXL protein, expressed from recombinant cDNA clones, were initially screened in vitro. CRISPR-Cas9 targeted mutagenesis and deletion of CCC CCA CCT CGC GCC TTC between exons 10 and 11 of murine *Axl* into the *C57BL/*6J background was performed in collaboration with the Transgenic and Targeted Mutagenesis Laboratory at Feinberg School of Medicine at Northwestern University with Dr. Lynn Doglio, Dr. Rajeshwar Awatramani, and Dr. Pei-Ken Hsu. This specifically deleted a 6 amino acid region within a 14 amino acid stalk region proximal to the transmembrane domain of AXL to generate cleavage-resistant AXL mice (*AxlCR/CR*). The male founder Axl-Del2 #6598 was born on 07/18/17 and

genotyping confirmed the presence of the correct allele. PCR genotyping primer oligonucleotides for *AxlCR/CR* genotyping are as follows: Axl-saF: ACT CAC TGG TCA TTC CAC ACC and Axl-saR: CCA TGA CTT CAG CTT CCC CG. See Supplemental Methods for full genotyping protocol.

Myocardial Reperfused Infarction: Surgeries were performed on female mice aged 2-4 months of age. Mice were anesthetized with avertin (2,2,2-Tribromoethanol, 99%, 0.1 mg/kg i.p.) and received sustained-release buprenorphine (0.1 mg/kg s.c.) prior to the first incision. Puralube Vet Ointment (Dechra) was applied to the eyes and mice were secured in a supine position and endotracheal-intubated to an Inspira Advanced Safety Single Animal Pressure/Volume Controlled Ventilator (Harvard Apparatus). Animals were maintained at 37°C using a far infrared warming pad (Kent Scientific) and animal temperature was monitored throughout surgery by a rectal probe using a MircoTherma 2 meter (ThermoWorks). Using a Leica S4E dissecting microscope and ACE Light Source (Schott), a left thoracotomy was performed with the aid of a Geiger Thermal Cautery Unit (Delasco) to maintain normal hemostasis. The left ventricle was visualized and the proximal left anterior descending (LAD) coronary artery was temporarily ligated with Surgipro II 7-0 monofilament polypropylene sutures (Covidien) approximately 2 mm distal to the site of its emergence from under the left atrium. Flexible plastic tubing (Tygon) was used during ligation to preserve the integrity of the vessel. Blanching/pale discoloration and hypokinesis of the anterior wall verified ligation. During ischemia, animal anesthesia was continuously monitored and additional avertin was administered following a positive toe pinch response. Following 45 minutes of ischemia, the ligature was reopened to allow for reperfusion. The reopened ligature was left in place to aid future analyses of infarct tissue. Reperfusion was confirmed by restoration of blood flow in the LAD and return of color to the left ventricle. Using Surgipro II 6-0 monofilament polypropylene sutures (Covidien), the surgical site was closed in layers starting with the chest wall followed by the pectoral muscle and finally skin and subcutaneous tissue. Animals were

allowed to recover on a heating pad (Sunbeam) prior to being returned to cages. Mice dying within 48 hours of surgery were treated as technical errors and excluded from analyses.

Statistics: Analyses were performed with GraphPad Prism 9 software (GraphPad Software). Comparisons between two groups were performed using two-tailed, unpaired t-test with 95% confidence interval. For comparisons of more than two variables, One-Way ANOVA or Two-Way ANOVA was utilized with 95% confidence interval and when necessary, Tukey test was used to correct for multiple comparisons. For in vivo experiments, experimental sample size is depicted in figures and represent pooled data from 2 or more independent experiments. For in vitro experiments, experimental sample size is depicted in figures and represent 2 or more independent experiments. Data are presented as mean ± SEM. Criteria for significant differences (*p<0.05, **p<0.01, ***p<0.001) are located in figure legends. Analyses labeled ns are not statistically significant.

Study Approval: These studies were approved by the Institutional Review Board at Northwestern University and performed in accordance with the Helsinki Doctrine on Human Experimentation. Written consent was obtained from all study participants. Animal studies were conducted in accordance with guidelines using a protocol approved by the Institutional Animal Care and Use Committee at Northwestern University.

A complete description of methods is provided in Supplemental Methods.

AUTHOR CONTRIBUTIONS

MD and EBT designed the research studies. MD and KG conducted experiments and acquired data. CVR generated and provided the *Axl*^{flox} mice. MS and IT performed initial screenings to identify AXL cleavage-resistant mutants. LDW provided the human myocardial specimens. All authors contributed to data analyses. MD and EBT wrote the manuscript, and all authors contributed to manuscript revision.

ACKNOWLEDGMENTS

This work was supported by AHA CDA24110032 (to MPD) and NIH grants F32HL127958 (to MPD), R01HL122309 and R01HL139812 (to EBT), R35HL145228 (IT), and R01HL127464 (IT). These studies used CRISPR/Cas9 gene editing services provided by the Transgenic and Targeted Mutagenesis Laboratory at Feinberg School of Medicine at Northwestern University. We are thankful to Anna Huskin, RN, BSN, CCRC, Program Development Manager in the Clinical Trials Unit of the Bluhm Cardiovascular Institute and Patrick McCarthy, MD, the Executive Director of the Bluhm Cardiovascular Institute.

REFERENCES

1. DeBerge M, Shah SJ, Wilsbacher L, and Thorp EB. Macrophages in Heart Failure with Reduced versus Preserved Ejection Fraction. *Trends in Molecular Medicine.* 2019;25(4):328-40.
2. Adamo L, Rocha-Resende C, Prabhu SD, and Mann DL. Reappraising the role of inflammation in heart failure. *Nature Reviews Cardiology.* 2020;17(5):269-85.
3. King KR, Aguirre AD, Ye Y-X, Sun Y, Roh JD, Ng RP, et al. IRF3 and type I interferons fuel a fatal response to myocardial infarction. *Nature Medicine.* 2017;23(12):1481-7.
4. Huang S, and Frangogiannis NG. Anti-inflammatory therapies in myocardial infarction: failures, hopes and challenges. *British Journal of Pharmacology.* 2018;175(9):1377-400.
5. Ridker PM, Everett BM, Thuren T, MacFadyen JG, Chang WH, Ballantyne C, et al. Antiinflammatory Therapy with Canakinumab for Atherosclerotic Disease. *New England Journal of Medicine.* 2017;377(12):1119-31.
6. Zagórska A, Través PG, Lew ED, Dransfield I, and Lemke G. Diversification of TAM receptor tyrosine kinase function. *Nature Immunology.* 2014;15(10):920-8.
7. Rothlin CV, Ghosh S, Zuniga EI, Oldstone MBA, and Lemke G. TAM Receptors Are Pleiotropic Inhibitors of the Innate Immune Response. *Cell.* 2007;131(6):1124-36.
8. Cai B, Thorp EB, Doran AC, Subramanian M, Sansbury BE, Lin C-S, et al. MerTK cleavage limits proresolving mediator biosynthesis and exacerbates tissue inflammation. *Proceedings of the National Academy of Sciences.* 2016;113(23):6526.
9. Cai B, Thorp EB, Doran AC, Sansbury BE, Daemen MJAP, Dorweiler B, et al. MerTK receptor cleavage promotes plaque necrosis and defective resolution in atherosclerosis. *The Journal of Clinical Investigation.* 2017;127(2):564-8.
10. Wan E, Yeap Xin Y, Dehn S, Terry R, Novak M, Zhang S, et al. Enhanced Efferocytosis of Apoptotic Cardiomyocytes Through Myeloid-Epithelial-Reproductive Tyrosine Kinase Links Acute Inflammation Resolution to Cardiac Repair After Infarction. *Circulation Research.* 2013;113(8):1004-12.
11. Howangyin K-Y, Zlatanova I, Pinto C, Ngkelo A, Cochain C, Rouanet M, et al. Myeloid-Epithelial-Reproductive Receptor Tyrosine Kinase and Milk Fat Globule Epidermal Growth Factor 8 Coordinately Improve Remodeling After Myocardial Infarction via Local Delivery of Vascular Endothelial Growth Factor. *Circulation.* 2016;133(9):826-39.
12. DeBerge M, Yeap Xin Y, Dehn S, Zhang S, Grigoryeva L, Misener S, et al. MerTK Cleavage on Resident Cardiac Macrophages Compromises Repair After Myocardial Ischemia Reperfusion Injury. *Circulation Research.* 2017;121(8):930-40.
13. Batlle M, Recarte-Pelz P, Roig E, Castel MA, Cardona M, Farrero M, et al. AXL receptor tyrosine kinase is increased in patients with heart failure. *International Journal of Cardiology.* 2014;173(3):402-9.
14. Caldentey G, García De Frutos P, Cristóbal H, Garabito M, Berruezo A, Bosch X, et al. Serum levels of Growth Arrest-Specific 6 protein and soluble AXL in patients with ST-segment elevation myocardial infarction. *European Heart Journal: Acute Cardiovascular Care.* 2017;8(8):708-16.
15. Heng TSP, Painter MW, Elpek K, Lukacs-Kornek V, Mauermann N, Turley SJ, et al. The Immunological Genome Project: networks of gene expression in immune cells. *Nature Immunology.* 2008;9(10):1091-4.
16. Zagórska A, Través PG, Jiménez-García L, Strickland JD, Oh J, Tapia FJ, et al. Differential regulation of hepatic physiology and injury by the TAM receptors Axl and Mer. *Life Science Alliance.* 2020;3(8):e202000694.
17. Lantz C, Radmanesh B, Liu E, Thorp EB, and Lin J. Single-cell RNA sequencing uncovers heterogenous transcriptional signatures in macrophages during efferocytosis. *Scientific Reports.* 2020;10(1):14333.

18. Batchu SN, Xia J, Ko KA, Doyley MM, Abe J-I, Morrell CN, et al. Axl modulates immune activation of smooth muscle cells in vein graft remodeling. *American Journal of Physiology-Heart and Circulatory Physiology.* 2015;309(6):H1048-H58.
19. Schmid ET, Pang IK, Carrera Silva EA, Bosurgi L, Miner JJ, Diamond MS, et al. AXL receptor tyrosine kinase is required for T cell priming and antiviral immunity. *eLife.* 2016;5:e12414.
20. Chakarov S, Lim HY, Tan L, Lim SY, See P, Lum J, et al. Two distinct interstitial macrophage populations coexist across tissues in specific subtissular niches. *Science.* 2019;363(6432):eaau0964.
21. Epelman S, Lavine Kory J, Beaudin Anna E, Sojka Dorothy K, Carrero Javier A, Calderon B, et al. Embryonic and Adult-Derived Resident Cardiac Macrophages Are Maintained through Distinct Mechanisms at Steady State and during Inflammation. *Immunity.* 2014;40(1):91-104.
22. Zhang W, Lavine Kory J, Epelman S, Evans Sarah A, Weinheimer Carla J, Barger Philip M, et al. Necrotic Myocardial Cells Release Damage-Associated Molecular Patterns That Provoke Fibroblast Activation In Vitro and Trigger Myocardial Inflammation and Fibrosis In Vivo. *Journal of the American Heart Association.* 2015;4(6):e001993.
23. Tannahill GM, Curtis AM, Adamik J, Palsson-McDermott EM, McGettrick AF, Goel G, et al. Succinate is an inflammatory signal that induces IL-1β through HIF-1α. *Nature.* 2013;496(7444):238-42.
24. Cramer T, Yamanishi Y, Clausen BE, Förster I, Pawlinski R, Mackman N, et al. HIF-1α Is Essential for Myeloid Cell-Mediated Inflammation. *Cell.* 2003;112(5):645-57.
25. Parra-Izquierdo I, Castaños-Mollor I, López J, Gómez C, San Román JA, Sánchez Crespo M, et al. Lipopolysaccharide and interferon-γ team up to activate HIF-1α via STAT1 in normoxia and exhibit sex differences in human aortic valve interstitial cells. *Biochimica et Biophysica Acta (BBA) - Molecular Basis of Disease.* 2019;1865(9):2168-79.
26. Joshi VD, Kalvakolanu DV, Chen W, Zhang L, Kang TJ, Thomas KE, et al. A Role for Stat1 in the Regulation of Lipopolysaccharide-Induced Interleukin-1β Expression. *Journal of Interferon & Cytokine Research.* 2006;26(10):739-47.
27. Holland SJ, Pan A, Franci C, Hu Y, Chang B, Li W, et al. R428, a Selective Small Molecule Inhibitor of Axl Kinase, Blocks Tumor Spread and Prolongs Survival in Models of Metastatic Breast Cancer. *Cancer Research.* 2010;70(4):1544.
28. Seitz HM, Camenisch TD, Lemke G, Earp HS, and Matsushima GK. Macrophages and Dendritic Cells Use Different Axl/Mertk/Tyro3 Receptors in Clearance of Apoptotic Cells. *The Journal of Immunology.* 2007;178(9):5635.
29. Bárcena C, Stefanovic M, Tutusaus A, Joannas L, Menéndez A, García-Ruiz C, et al. Gas6/Axl pathway is activated in chronic liver disease and its targeting reduces fibrosis via hepatic stellate cell inactivation. *Journal of Hepatology.* 2015;63(3):670-8.
30. Shibata T, Habiel DM, Coelho AL, Kunkel SL, Lukacs NW, and Hogaboam CM. Axl Receptor Blockade Ameliorates Pulmonary Pathology Resulting from Primary Viral Infection and Viral Exacerbation of Asthma. *The Journal of Immunology.* 2014;192(8):3569.
31. Fujimori T, Grabiec AM, Kaur M, Bell TJ, Fujino N, Cook PC, et al. The Axl receptor tyrosine kinase is a discriminator of macrophage function in the inflamed lung. *Mucosal Immunology.* 2015;8(5):1021-30.
32. Shibata T, Makino A, Ogata R, Nakamura S, Ito T, Nagata K, et al. Respiratory syncytial virus infection exacerbates pneumococcal pneumonia via Gas6/Axl-mediated macrophage polarization. *The Journal of Clinical Investigation.* 2020;130(6):3021-37.
33. Espindola MS, Habiel DM, Narayanan R, Jones I, Coelho AL, Murray LA, et al. Targeting of TAM Receptors Ameliorates Fibrotic Mechanisms in Idiopathic Pulmonary Fibrosis. *American Journal of Respiratory and Critical Care Medicine.* 2018;197(11):1443-56.

34. De S, Zhou H, DeSantis D, Croniger CM, Li X, and Stark GR. Erlotinib protects against LPS-induced Endotoxicity because TLR4 needs EGFR to signal. *Proceedings of the National Academy of Sciences.* 2015;112(31):9680.
35. Paccez JD, Vasques GJ, Correa RG, Vasconcellos JF, Duncan K, Gu X, et al. The receptor tyrosine kinase Axl is an essential regulator of prostate cancer proliferation and tumor growth and represents a new therapeutic target. *Oncogene.* 2013;32(6):689-98.
36. Son B-K, Kozaki K, Iijima K, Eto M, Nakano T, Akishita M, et al. Gas6/Axl-PI3K/Akt pathway plays a central role in the effect of statins on inorganic phosphate-induced calcification of vascular smooth muscle cells. *European Journal of Pharmacology.* 2007;556(1):1-8.
37. Cruz VH, Arner EN, Du W, Bremauntz AE, and Brekken RA. Axl-mediated activation of TBK1 drives epithelial plasticity in pancreatic cancer. *JCI Insight.* 2019;4(9).
38. Tugal D, Liao X, and Jain Mukesh K. Transcriptional Control of Macrophage Polarization. *Arteriosclerosis, Thrombosis, and Vascular Biology.* 2013;33(6):1135-44.
39. Han J, Bae J, Choi C-Y, Choi S-P, Kang H-S, Jo E-K, et al. Autophagy induced by AXL receptor tyrosine kinase alleviates acute liver injury via inhibition of NLRP3 inflammasome activation in mice. *Autophagy.* 2016;12(12):2326-43.
40. Rankin EB, Fuh KC, Castellini L, Viswanathan K, Finger EC, Diep AN, et al. Direct regulation of GAS6/AXL signaling by HIF promotes renal metastasis through SRC and MET. *Proceedings of the National Academy of Sciences.* 2014;111(37):13373.
41. Zhen Y, Priest SO, and Shao W-H. Opposing Roles of Tyrosine Kinase Receptors Mer and Axl Determine Clinical Outcomes in Experimental Immune-Mediated Nephritis. *The Journal of Immunology.* 2016;197(6):2187.
42. Subramanian M, Proto JD, Matsushima GK, and Tabas I. Deficiency of AXL in Bone Marrow-Derived Cells Does Not Affect Advanced Atherosclerotic Lesion Progression. *Scientific Reports.* 2016;6(1):39111.
43. Zhang S, Weinberg S, DeBerge M, Gainullina A, Schipma M, Kinchen JM, et al. Efferocytosis Fuels Requirements of Fatty Acid Oxidation and the Electron Transport Chain to Polarize Macrophages for Tissue Repair. *Cell Metabolism.* 2019;29(2):443-56.e5.
44. Loges S, Gjertsen BT, Heuser M, Ben-Batalla I, Micklem D, Jorg C, et al. A first-in-patient phase I study of BGB324, a selective Axl kinase inhibitor in patients with refractory/relapsed AML and high-risk MDS. *Journal of Clinical Oncology.* 2016;34(15_suppl):2561-.
45. Scott RS, McMahon EJ, Pop SM, Reap EA, Caricchio R, Cohen PL, et al. Phagocytosis and clearance of apoptotic cells is mediated by MER. *Nature.* 2001;411(6834):207-11.
46. Lu Q, Gore M, Zhang Q, Camenisch T, Boast S, Casagranda F, et al. Tyro-3 family receptors are essential regulators of mammalian spermatogenesis. *Nature.* 1999;398(6729):723-8.

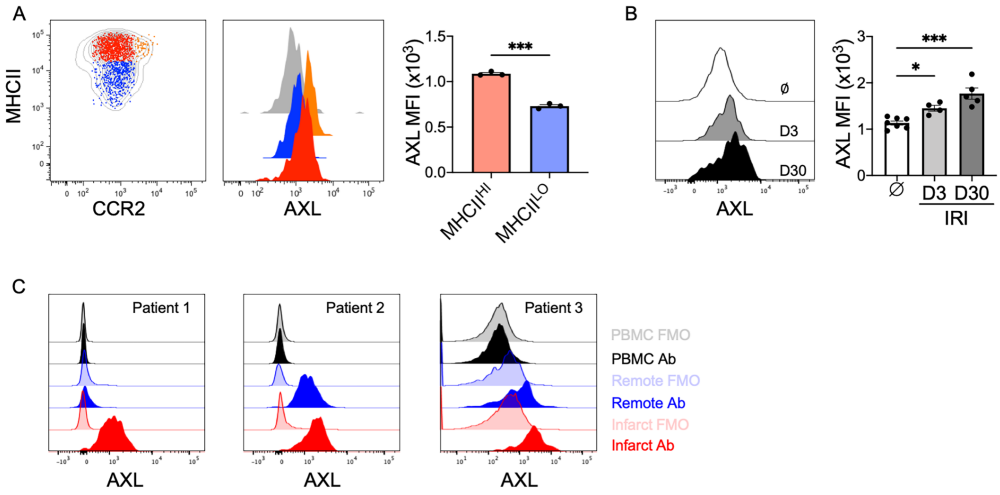

Figure 1: AXL expression is increased on human and murine macrophages after myocardial ischemia-reperfused infarction (IRI). A Cell-surface protein expression of AXL on different cardiac macrophage subsets with quantification of AXL expression on MHCII^{HI}CCR2^{-} (red) and MHCII^{LO}CCR2^{-} (blue) macrophages. The gray histogram represents *Axl-/-* cardiac macrophage staining control. Data represent mean ± SEM and are representative of 3 independent experiments. n=3 mice/group. ***p<0.001, 2-tailed unpaired t test. **B** AXL expression on murine cardiac macrophages before and 3 or 30 days after myocardial IRI. Data represent mean ± SEM. n=4-7 mice/group pooled from 2 independent experiments. *p<0.05, ***p<0.001, 1-way ANOVA followed by Tukey's test. **C** Expression of AXL on peripheral blood mononuclear cells (PBMC) or human cardiac macrophages isolated from peri-infarct or remote tissue from the explanted hearts of patients with ischemic cardiomyopathy at the time of heart transplantation. Fluorescence minus one (FMO) was used as a staining control.

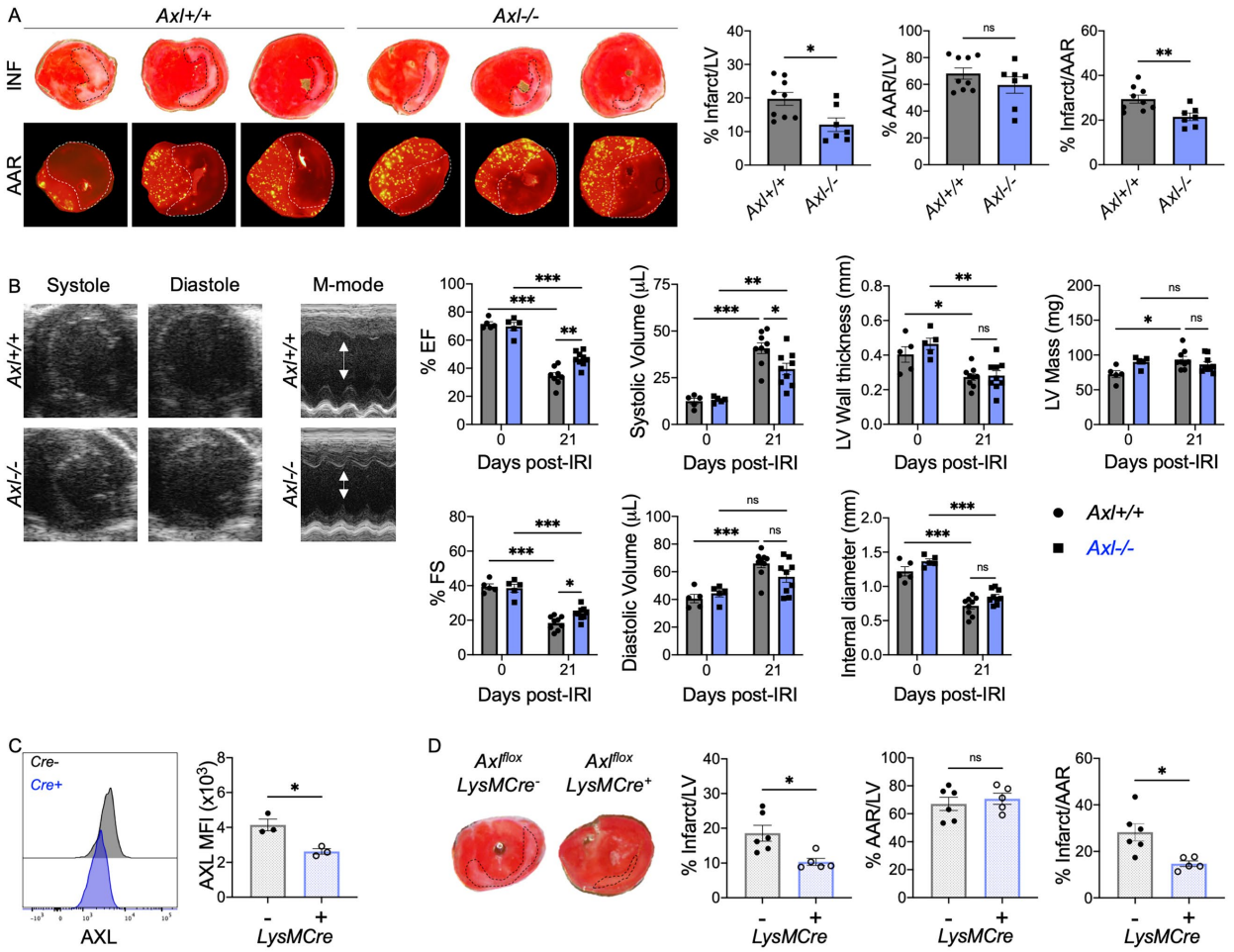

Figure 2: Macrophage AXL worsens cardiac repair after myocardial ischemia-reperfused infarction (IRI). A Representative 1 mm heart sections from an individual *Axl+/+* or *Axl-/-* mouse 7 days after IRI stained with triphenyltetrazolium chloride (TTC) for infarct measurements or injected with fluorescent microspheres to quantify the area-at-risk (AAR). From left to right, apex towards the ligation site. Percent Infarct/Left Ventricle (LV), percent AAR/LV, and percent Infarct/AAR measured 7 days after IRI in mice with whole body deletion of *Axl*. Data represent mean ± SEM. n=7-9 mice/group pooled from 3 independent experiments. **p*<0.05, ***p*<0.01, 2-tailed unpaired *t* test. **B** Representative B-mode and M-mode echocardiography images of systole and diastole in hearts 21 days after IRI with quantification of percent ejection fraction (% EF), percent fractional shortening (% FS), systolic and diastolic volume, LV wall thickness, internal

diameter, and LV mass 21 days after IRI. Data represent mean ± SEM. n=5-9 mice/group pooled from 2 independent experiments. *p<0.05, **p<0.01, ***p<0.001, 2-way ANOVA followed by Tukey's test. **C** AXL expression on cardiac macrophages in mice with myeloid-specific deletion of *Axl* (*LysMCre*$^{+}$*Axl*^{flox}) as measured by flow cytometry. Data represent mean ± SEM and are representative of 2 independent experiments. n=3 mice/group. *p<0.05, 2-tailed unpaired *t* test. **D** Infarct measurements 7 days after IRI in *LysMCre*$^{+}$*Axl*^{flox} mice compared to *LysMCre*$^{-}$*Axl*^{flox} littermate controls. Data represent mean ± SEM. n=5-6 mice/group pooled from 2 independent experiments. *p<0.05, 2-tailed unpaired *t* test.

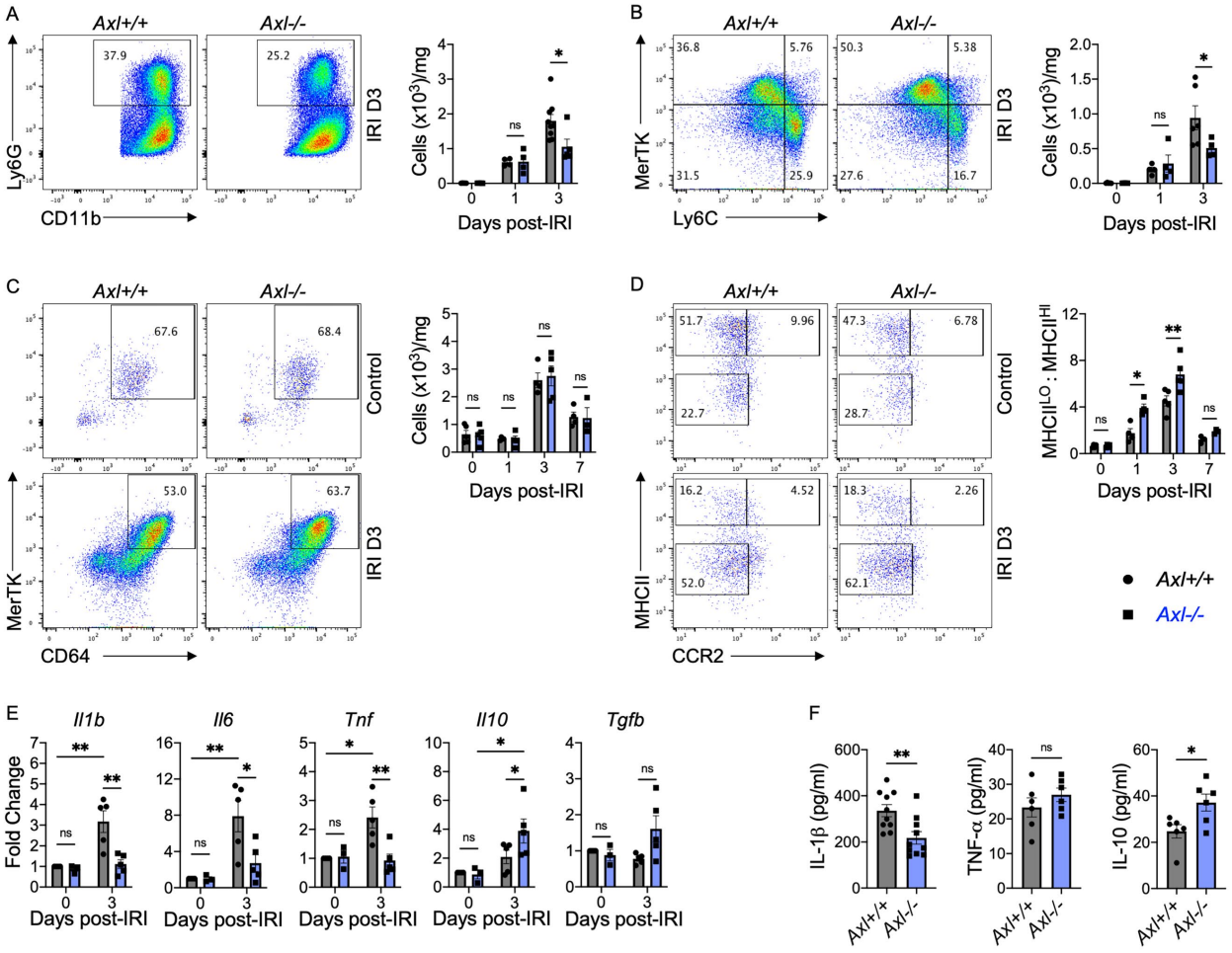

Figure 3: Macrophage AXL promotes inflammatory responses after myocardial ischemia-reperfused infarction (IRI). Total number of **A** neutrophils and **B** Ly6C^{hi} monocytes within the infarcted myocardium as measured on the days indicated after IRI in *Axl+/+* or *Axl-/-* mice. Flow plots depict events 3 days after IRI. **C** Total number of MerTK^{+} macrophages within the infarcted myocardium as measured on the indicated days after IRI in *Axl+/+* or *Axl-/-* mice. **D** Ratio of MHCII^{LO} to MHCII^{HI} macrophages (MΦ) within the infarcted myocardium as measured on the days indicated after IRI in *Axl+/+* or *Axl-/-* mice. For **A**, **B**, **C**, and **D**, data represent mean ± SEM. n=4-5 mice/group pooled from 3 independent experiments. *p<0.05, **p<0.01, 2-way ANOVA followed by Tukey's test. **E** Gene expression of pro- and anti-inflammatory mediators in whole infarct extracts from *Axl+/+* or *Axl-/-* mice. Data represent mean ± SEM. n=3-5 mice/group pooled from 3 independent experiments. *p<0.05, **p<0.01, 2-way ANOVA followed by Tukey's test. **F** Serum

levels of pro- and anti-inflammatory mediators as measured 3 days after IRI from in *Axl*+/+ or *Axl*-/- mice. Data represent mean ± SEM. n=6-10 mice/group pooled from 3 independent experiments. *$p<0.05$, **$p<0.01$, 2-tailed unpaired *t* test.

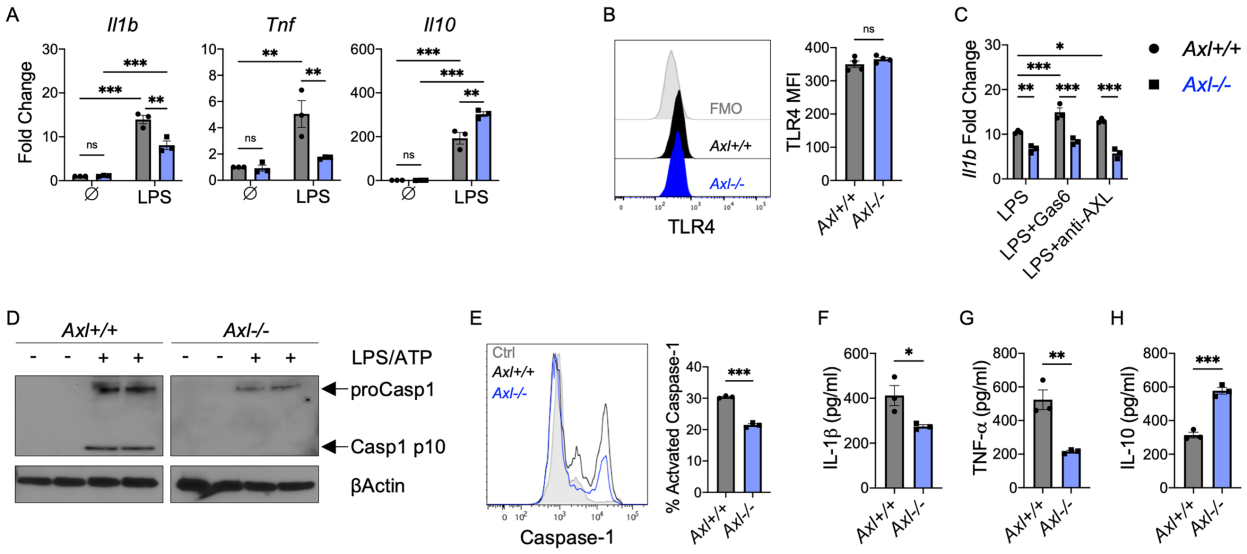

Figure 4: AXL signaling augments TLR4 priming of the inflammasome in macrophages. **A** Pro- and anti-inflammatory gene expression in *Axl+/+* or *Axl-/-* bone marrow-derived macrophages (BMDM) treated with lipopolysaccharide (LPS) for 6 hours. Data represent mean ± SEM and are representative of more than 3 independent experiments. n=3 sets of cells/group. ***p*<0.01, ****p*<0.001, 2-way ANOVA followed by Tukey's test. **B** TLR4 expression on untreated *Axl+/+* or *Axl-/-* BMDMs as measured by flow cytometry. Data represent mean ± SEM and are representative of 2 independent experiments. n=4 sets of cells/group. ns=not significant, 2-tailed unpaired *t* test. **C** Gene expression of *Il1b* in serum-starved *Axl+/+* or *Axl-/-* BMDMs treated with LPS and AXL-specific agonists, Growth arrest-specific 6 (Gas6) protein or anti-mouse AXL agonizing antibody, for 6 hours. Data represent mean ± SEM and are representative of 3 independent experiments. n=3 sets of cells/group. **p*<0.05, ***p*<0.01, ****p*<0.001, 2-way ANOVA followed by Tukey's test. **D** Immunoblot or **E** flow cytometry of caspase-1 activation in *Axl+/+* or *Axl-/-* BMDMs primed with LPS for 3 hours followed by activation with ATP for 30 minutes. Data represent mean ± SEM and are representative of 3 independent experiments. n=2-3 sets of cells/group. ****p*<0.001, 2-tailed unpaired *t* test. **F** IL-1β production by *Axl+/+* or *Axl-/-* BMDMs primed with LPS for 3 hours followed by activation with ATP for 30 minutes. **G** TNF-α or **H** IL-10 production by *Axl+/+* or *Axl-/-* BMDMs treated with LPS for 6 hours. For **F**, **G**, and **H**, data

represent mean ± SEM and are representative of more than 3 independent experiments. n=3 sets of cells/group. *p<0.05, **p<0.01, ***p<0.001, 2-tailed unpaired t test.

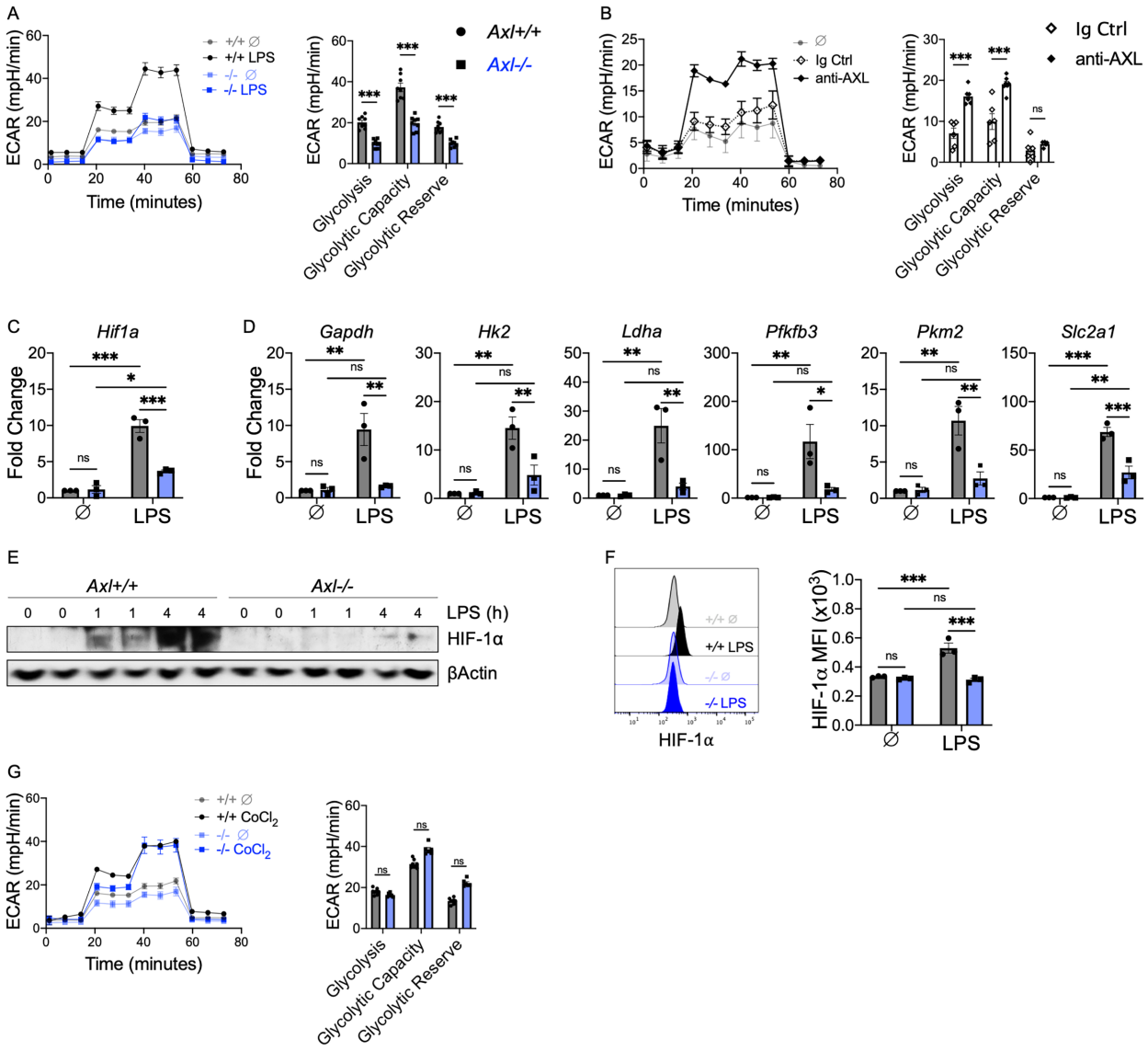

Figure 5: AXL signaling is required for a switch to glycolytic metabolism to fuel proinflammatory responses in macrophages. A Extracellular acidification rate (ECAR) in *Axl+/+* or *Axl-/-* bone marrow-derived macrophages (BMDM) treated with lipopolysaccharide (LPS) for 3 hours with quantification of glycolytic function. **B** ECAR with quantification of glycolytic function in *Axl+/+* BMDMs treated with anti-mouse AXL agonizing antibody or isotype control. For **A** and **B**, data represent mean ± SEM and are representative of two to three independent experiments. n=5-8 sets of cells/group. ***p<0.001, 2-tailed unpaired t test. **C** *Hif1a* gene expression in BMDMs treated with LPS for 3 hours. **D** Expression of genes involved in glycolytic

metabolism in BMDMs treated with LPS for 3 hours. For **C** and **D**, data represent mean ± SEM and are representative of two independent experiments. n=3 sets of cells/group. *p<0.05, **p<0.01, ***p<0.001, 2-way ANOVA followed by Tukey's test. **E** Immunoblot or **F** flow cytometry of HIF-1α protein in BMDMs treated with LPS. Data represent mean ± SEM and are representative of 2 independent experiments. n=3 sets of cells/group. ***p<0.001, 2-way ANOVA followed by Tukey's test. **G** ECAR with quantification of glycolytic function measured in *Axl*+/+ or *Axl*-/- BMDMs treated with the HIF-1α pharmacological activator, cobalt chloride ($CoCl_2$). Untreated groups (+/+ Ø and -/- Ø) are the same as presented in panel **A**. Data represent mean ± SEM and are representative of two independent experiments. n=6-8 sets of cells/group. ns=not significant, 2-tailed unpaired *t* test.

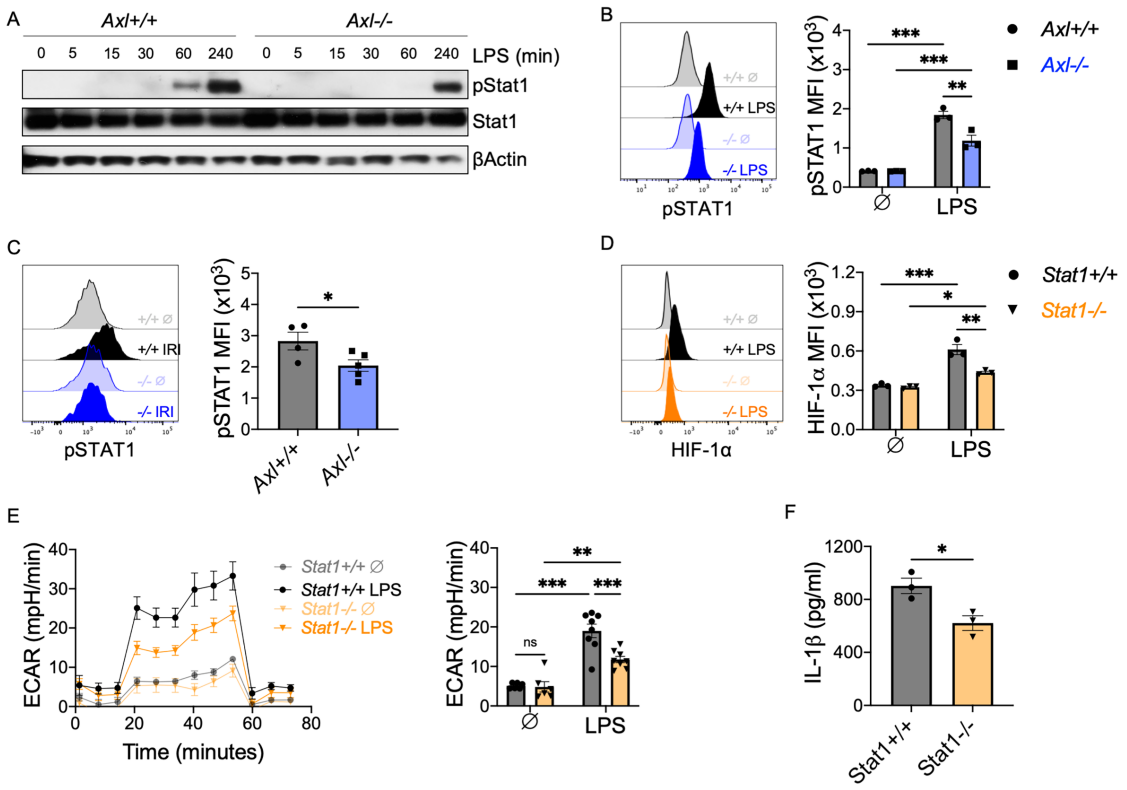

Figure 6: Cross signaling between AXL and TLR4 augments STAT1 activation to fuel proinflammatory responses in macrophages. A Immunoblot or **B** flow cytometry of STAT1 phosphorylation in *Axl+/+* or *Axl-/-* bone marrow-derived macrophages (BMDM) treated with lipopolysaccharide (LPS). Data represent mean ± SEM and are representative of two to three independent experiments. n=3 sets of cells/group. ***p*<0.01, ****p*<0.001, 2-way ANOVA followed by Tukey's test. **C** STAT1 phosphorylation in *Axl+/+* or *Axl-/-* cardiac macrophages 3 days after ischemia-reperfusion infarction (IRI). Data represent mean ± SEM. n=4-5 mice/group pooled from 2 independent experiments. **p*<0.05, 2-tailed unpaired *t* test. **D** HIF-1α protein in *Stat1+/+* or *Stat1-/-* BMDMs treated with LPS for 4 hours as measured by flow cytometry. Data represent mean ± SEM and are representative of 2 independent experiments. n=3 sets of cells/group. **p*<0.05, ***p*<0.01, ****p*<0.001, 2-way ANOVA followed by Tukey's test. **E** Extracellular acidification rate (ECAR) with quantification of glycolytic function in *Stat1+/+* or *Stat1-/-* BMDMs treated with LPS for 3 hours. Data represent mean ± SEM and are representative of two

independent experiments. n=6-8 sets of cells/group. *p<0.05, ***p<0.001, 2-way ANOVA followed by Tukey's test. **F** IL-1β production by *Stat1+/+* or *Stat1-/-* BMDMs primed with LPS for 3 hours followed by activation with ATP for 30 minutes. Data represent mean ± SEM and are representative of two independent experiments. n=3 sets of cells/group. *p<0.05, 2-tailed unpaired *t* test.

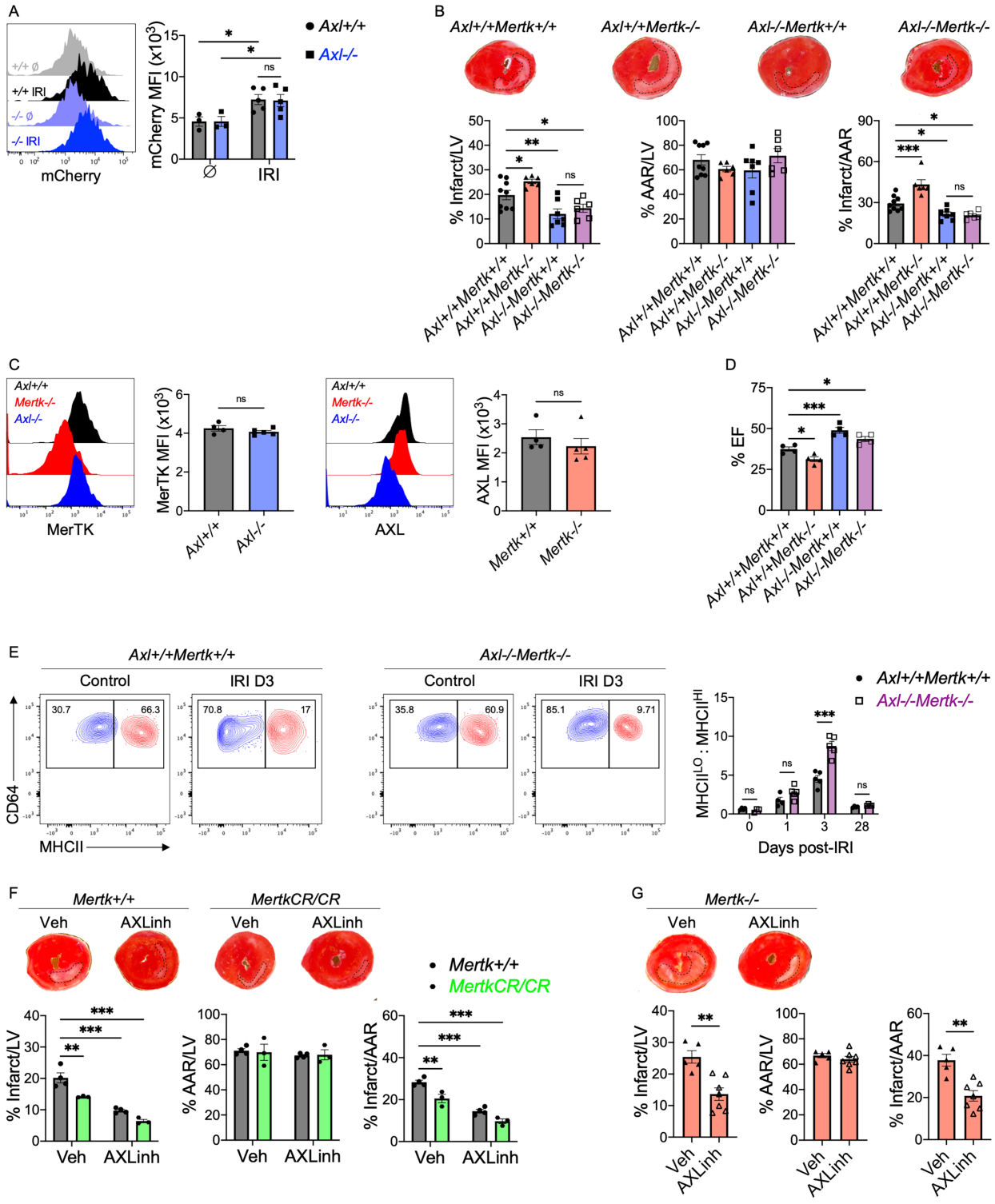

Figure 7: Divergent roles for AXL and MerTK in cardiac repair after myocardial ischemia-reperfused infarction (IRI). A Phagocytosis of apoptotic mCherry-expressing cardiomyocytes by

cardiac macrophages from *Axl+/+* or *Axl-/-* mice at baseline or 4 hours after IRI. Data represent mean ± SEM. n=3-5 mice/group pooled from 3 independent experiments. **p*<0.05, 2-way ANOVA followed by Tukey's test. **B** Percent Infarct/Left Ventricle (LV), percent Area-at-Risk (AAR)/LV, percent Infarct/AAR measured 7 days after IRI in mice lacking either *Mertk* (*Axl+/+Mertk-/-*), *Axl* (*Axl-/-Mertk+/+*), or both *Mertk* and *Axl* (*Axl-/-Mertk-/-*). Data represent mean ± SEM. n=6-9 mice/group pooled from more than 3 independent experiments. **p*<0.05, ***p*<0.01, ****p*<0.001, 1-way ANOVA followed by Tukey's test. **C** Expression of MerTK and AXL on cardiac macrophages from *Axl-* or *Mertk*-deficient mice as measured 3 days after IRI. Data represent mean ± SEM. n=4-5 mice/group pooled from 2 independent experiments. ns=not significant, 2-tailed unpaired *t* test. **D** Quantification of percent ejection fraction (% EF) in mice 28 days after IRI. Data represent mean ± SEM. n=4 mice/group pooled from 4 independent experiments. **p*<0.05, ****p*<0.001, 1-way ANOVA followed by Tukey's test. **E** Ratio of $MHCII^{LO}$ to $MHCII^{HI}$ cardiac macrophages within the infarcted myocardium of *Axl+/+Mertk+/+* or *Axl-/-Mertk-/-* mice. Data represent mean ± SEM. n=3-5 mice/group pooled from 3 independent experiments. ****p*<0.001, 2-way ANOVA followed by Tukey's test. **F** Infarct measurements 7 days after IRI in *Mertk+/+* or *MertkCR/CR* mice treated with the AXL selective inhibitor, R428, or vehicle. Data represent mean ± SEM. n=3-4 mice/group pooled from 3 independent experiments. ***p*<0.01, ****p*<0.001, 2-way ANOVA followed by Tukey's test. **G** Infarct measurements 7 days after IRI in *Mertk-/-* mice treated with the AXL selective inhibitor, R428, or vehicle. Data represent mean ± SEM. n=5-7 mice/group pooled from 3 independent experiments. ***p*<0.01, 2-tailed unpaired *t* test.

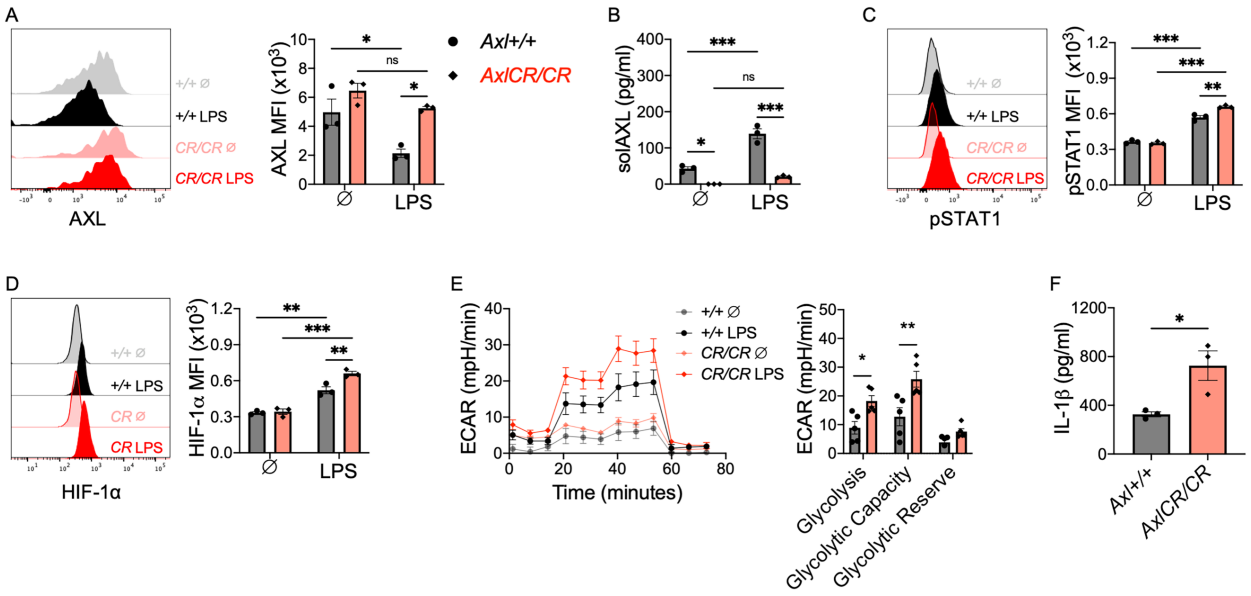

Figure 8: AXL cleavage limits proinflammatory responses in macrophages. A Cell surface expression of AXL on bone marrow-derived macrophages (BMDMs) from wild-type (*Axl+/+)* or AXL cleavage-resistant (*AxlCR/CR*) mice treated with lipopolysaccharide (LPS) for 1 hour. **B** Soluble AXL (solAXL) in culture media of BMDMs treated with LPS for 1 hour. **C** STAT1 phosphorylation in BMDMs treated with LPS for 1 hour. **D** HIF-1α protein in BMDMs treated with LPS for 4 hours. For **A**, **B**, **C**, and **D**, data represent mean ± SEM and are representative of 3 independent experiments. n=3 sets of cells/group. **p*<0.05, ***p*<0.01, ****p*<0.001, 2-way ANOVA followed by Tukey's test. **E** Extracellular acidification rate (ECAR) with quantification of glycolytic function in BMDMs treated with LPS for 3 hours. Data represent mean ± SEM and are representative of 2 independent experiments. n=5 sets of cells/group. **p*<0.05, ***p*<0.01, 2-tailed unpaired *t* test. **F** IL-1β production by BMDMs treated with LPS for 18 hours. Data represent mean ± SEM. n=3 sets of cells/group. **p*<0.05, 2-tailed unpaired *t* test.

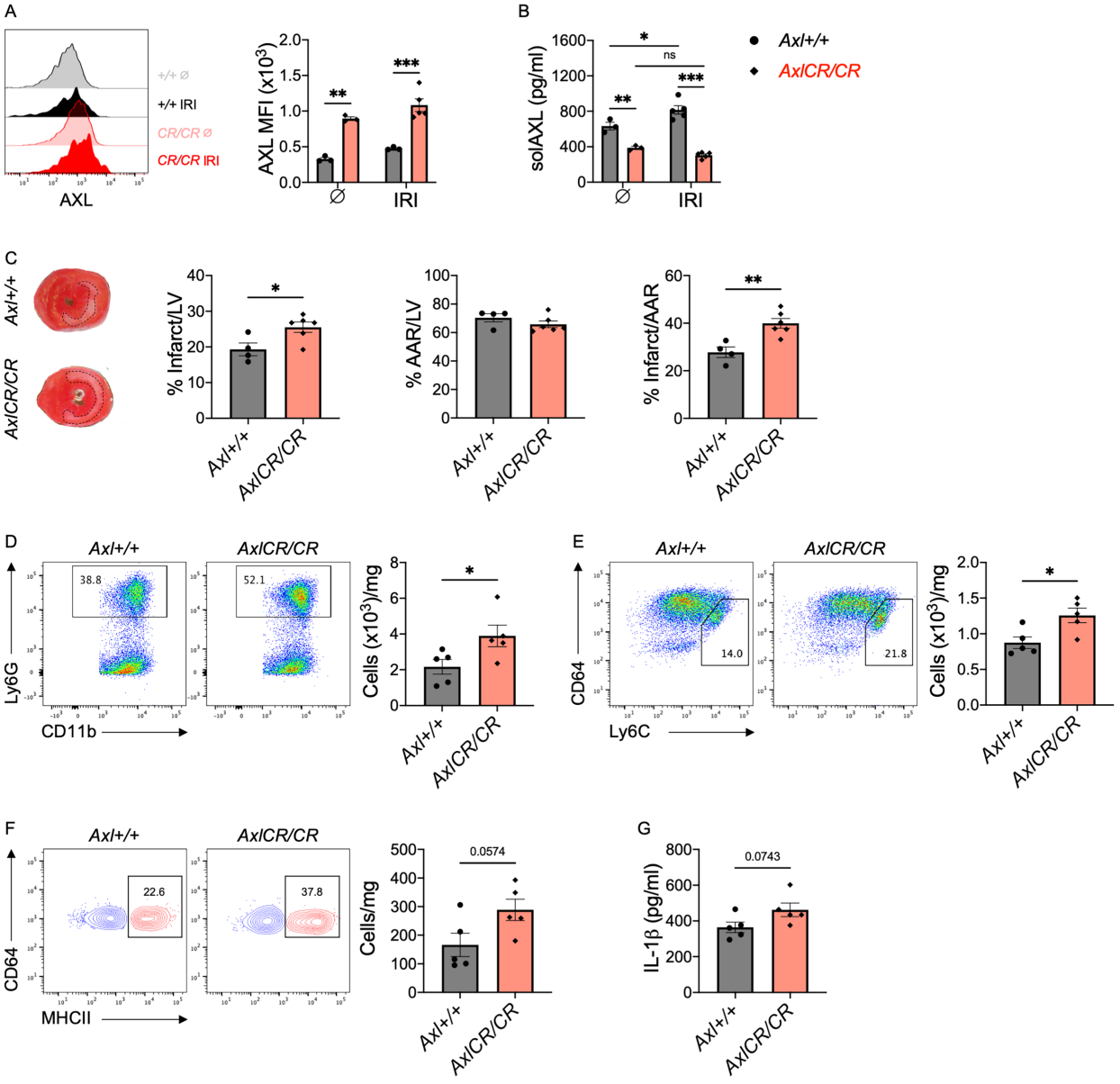

Figure 9: AXL cleavage limits adverse ventricular remodeling after myocardial ischemia-reperfused infarction (IRI). A Cell surface expression of AXL on cardiac macrophages from wild-type (*Axl+/+*) or AXL cleavage-resistant (*AxlCR/CR*) mice before or 3 days after IRI. **B** Serum levels of soluble AXL (solAXL) before or 3 days after IRI. For **A** and **B**, data represent data represent mean ± SEM. n=3-5 mice/group pooled from 3 independent experiments. **p*<0.05, ***p*<0.01, ****p*<0.001, 2-way ANOVA followed by Tukey's test. **C** Percent Infarct/Left Ventricle

(LV), percent Area-at-Risk (AAR)/LV, percent Infarct/AAR measured 7 days after IRI in *Axl*+/+ or *AxlCR/CR* mice. Data represent mean ± SEM. n=4-6 mice/group pooled from 3 independent experiments. *p<0.05, **p<0.01, 2-tailed unpaired t test. Total number of **D** neutrophils, **E** Ly6C^{hi} monocytes, and **F** MHCII^{HI} macrophages within the infarct 3 days after IRI. Flow plots depict events 3 days after IRI. **G** Serum levels of IL-1β as measured 3 days after IRI. For **D**, **E**, **F**, and **G**, data represent mean ± SEM. n=5 mice/group pooled from 2 independent experiments. *p<0.05, 2-tailed unpaired t test.